Synthesis challenges, thermodynamic stability, and growth kinetics of La-Si-P ternary compounds

Ling Tang[3], Weiyi Xia[1,4], Gayatri Viswanathan[1,2], Ernesto Soto[1,2], Kirill Kovnir[1,2], and Cai-Zhuang Wang[1,4,*]

[1]Ames National Laboratory, U.S. Department of Energy, Ames, IA 50011, United States.

[2]Department of Chemistry, Iowa State University, Ames, IA 50011, United States.

[3]School of Physics, Zhejiang University of Technology, Hangzhou, 310023, China

[4]Department of Physics and Astronomy, Iowa State University, Ames, IA 50011, United States

Corresponding author: * wangcz@ameslab.gov

Supplemental Materials

Experimental Methods

Warning: The vapor pressure of red phosphorus at high temperatures is significant and may be sufficient to compromise the integrity of sealed reaction ampoules. As such. the amount of phosphorus used for reactions should be kept to a minimum and it is highly recommended to place sealed ampoules in furnaces in a well-ventilated area, i.e. inside of a fumehood. Reaction ampoules may also be wrapped in ceramic wool casings, or cocoons, to contain damaged reactions and protect other ampoules in the furnace.

Arc-melting of P-containing samples may result in the release of toxic P vapor and substantial contamination of the arc-melting area with depositions of pyrophoric white phosphorus. It is highly recommended to limit arc-melting to samples with less than 25 at.% P and perform pre-annealing of such samples in sealed ampoules to bind P into less volatile metal phosphides.

Starting Materials. Lanthanum pieces (99.9999%, Ames National Lab, US DOE), silicon pieces (99.9999%, Ames National Lab, US DOE), silicon powder (99.99%, Alfa Aesar), red phosphorus powder (98.9%, Alfa Aesar), and cesium chloride (99.99%, Sigma Aldrich) were used as received. Lanthanum and silicon pieces were obtained from the Materials Preparation Center at Ames National Laboratory, which is supported by the US DOE Basic Energy Sciences. Reactions involving elemental lanthanum were prepared in an argon-filled glovebox (< 1 ppm O_2) to minimize oxidation. La pieces for arc melting were weighed inside the glovebox as well, then transported in an argon-filled vial to the arc melter.

Arc melting. Precursors with nominal composition "LaSi," "La_2Si," and "La_5Si_3" were prepared by arc-melting and used for solid state syntheses. Cut lanthanum and silicon pieces were weighed (total ~1g) in the nominal ratio with a 10% excess Si to account for evaporation during arc melting, e.g. $LaSi_{1.1}$ for a "LaSi" precursor. La and Si were placed on a copper hearth in an arc-melter along with zirconium metal as an oxygen getter. The chamber was sealed and evaluated for 20 min, then purged with argon thrice to ensure no oxygen was present. Zr metal was melted first to absorb any residual oxygen, then the precursor samples were arced ~30 sec at a current of I ~ 100 A until molten. Once solidified, the samples were flipped and arced twice at the former current to ensure homogeneity. The resulting ingots were crushed in an agate mortar, finely ground under hexanes, then dried prior to characterization by powder X-ray diffraction (PXRD) and being used for synthesis.

A similar procedure was followed for arc-melting La-Si-P reactions. It is not advisable to arc melt samples with red P, as it is a volatile species, and this would result in the contamination of the arc melter and deposition of pyrophoric white phosphorus. As such, pre-reacted samples containing P in the form of LaP were used as starting materials targeting predicted La-Si-P phases. Starting materials were finely ground into a powder under hexanes, dried, then cold-pressed into a small pellet (~120mg total) for arc melting.

Solid State Synthesis. Various syntheses were attempted to produce La_2SiP_3 (**Table S1-S3**). Reagents were weighed in the desired ratio, loaded in carbonized silica tubes, then sealed under

vacuum. For reactions involving arc-melted precursors and P, starting materials were ground in an agate mortar prior to loading in silica ampoules to improve homogeneity and reactivity. Ampoules were placed in a muffle furnace and heated in a temperature range of 1073-1423 K for 3-7 days. Reactions were opened on air, ground, then studied using PXRD. Selected reactions were further characterized by scanning electron microscopy and energy-dispersive X-ray spectroscopy (SEM/EDS) or differential scanning calorimetry (DSC). Reactions involving CsCl salt flux were washed briefly (<15 min) in DI water, filtered, then briefly dried on air prior to PXRD and additional characterization.

Powder X-ray Diffraction (PXRD). Diffraction data were collected on a Rigaku Miniflex 600 diffractometer with Cu-K_α radiation and a Ni-K_β filter. A thin layer of grease was applied to zero-background silicon holders, then sprinkled with sample powder.

Differential Scanning Calorimetry (DSC). A Netzsch DSC 404 Pegasus calorimeter was used for the DSC measurement. ~15mg of finely ground "La_2SiP_4" powder (LaP + La_2SiP_4) was loaded into a small silica ampoule and flame sealed under vacuum. The sealed ampoule was measured against an identical empty ampoule (reference). The sample was heated to 1373 K and cooled to room temperature at a rate of 10 K/min. After the experiment, the ampoule was opened and PXRD data was collected on the product.

Scanning Electron Microscopy and Energy Dispersive X-ray Spectroscopy (SEM/EDS). Backscattered electron images and semi-quantitative site compositions were obtained on a FEI Quanta 250 field-emission scanning electron microscope equipped with an EDS detector (Oxford X-Max 80, ThermoFischer Scientific, Inc., USA). Samples were prepped either by mounting powder on double-sided adhesive carbon tape or by mounting powders in epoxy, polishing to a level surface, and coating with a conductive layer of carbon. An accelerating voltage of 15 kV was applied for all measurements.

Table S1: Selected reactions targeting the formation of La_2SiP_3 using arc-melted precursors, CsCl salt flux, or both.

Starting Materials	Salt Flux	Ramp time	Dwell Temp., Duration	Major Products	Minor Products
5La + 3Si (1g)	-	-	Arc melted	**La_5Si_3 + La_5Si_4**	
2La + Si (1g)	-	-	Arc melted	**La_5Si_3**	La
2La + Si + 3P (200mg)	CsCl (2g)	10h	1073 K, 72h	**LaOCl**	LaP + $LaSiP_3$ *Aea*2
"La_5Si_3" + 7.5P (100mg)	-	10h	1073 K, 72h	**LaP**	$LaSiP_3$ *Aea*2
"La_5Si_3" + 7.5P (100mg)	CsCl (1g)	10h	1073 K, 72h	**LaP**	$LaSiP_3$ *Aea*2
"La_5Si_3" + 7.5P (100mg)	-	10h	1273 K, 72h	**LaP**	$LaSi_2$ + unindexed peaks
"La_5Si_3" + 7.5P (100mg)	CsCl (1g)	10h	1273 K, 72h	**LaP + unindexed peaks**	
"La_2Si" + 3P (100 mg)	-	14h	1423 K, 168h	**LaP**	$La_2Si_2O_7$ + unindexed peaks
"La_2Si" + 3P (45mg)	-	0h	1273 K, 140h	**LaP**	La_2SiP_4 + $La_2Si_2O_7$

Table S2: Selected reactions targeting the formation of La_2SiP or Si-doped LaP via arc melting.

Starting Materials	Ramp time	Dwell Temperature, Duration	Major Products	Minor Products
2La + Si	-	Arc melted	**La_5Si_3**	La
La + Si	-	Arc melted	**LaSi**	La_2Si_3
"La_2Si" + P (150mg)	10h	1273 K, 72h	**LaP**	LaSi + La_5Si_4 + La_2Si_3
"La_2SiP" (120mg)	-	Arc melted	**LaP** + LaSi	$LaSi_2$
0.8"LaSi" + 0.2"LaP" (120mg)	-	Arc melted	**La_2Si_3 + LaP** + LaSi	

Table S3: Selected reactions targeting the formation of La_2SiP_4 and its subsequent transformation to La_2SiP_3.

Starting Materials	Ramp time	Dwell Temperature, Duration	Major Products	Minor Products
2La + Si	-	Arc melted	**La_5Si_3**	La
"La_2Si" + 4P (100mg)	14h	1423 K, 168h	**LaP**	La_2SiP_4 + $La_2Si_2O_7$ $LaSiP_3$ *Aea*2
"La_2Si" + 4P (100mg)	14h	1273 K, 168h	**LaP**	La_2SiP_4
"La_2SiP_4" (80mg)	5h	1373 K, 120h – air quench	**LaP**	Unindexed peaks + $La_2Si_2O_7$

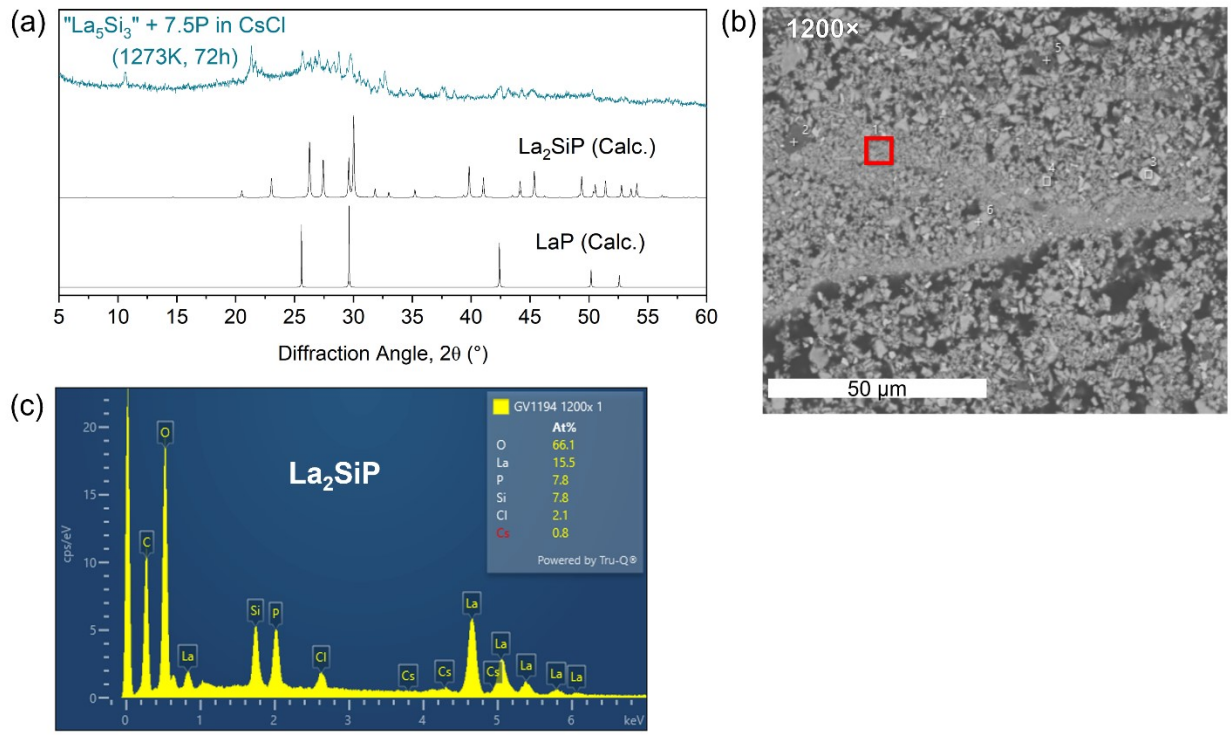

Fig. S1. **(a)** PXRD pattern (teal) of sample synthesized from La_5Si_3 precursor and P in CsCl salt flux at 1273 K. The sample was washed with DI water to remove the flux prior to PXRD. LaP is present as well as unindexed diffraction peaks. **(b)** Backscattered electron SEM image of epoxy-mounted powder of the sample. **(c)** EDS spectrum for the region outlined in red in **(b)**, corresponding to normalized composition of La_2SiP, or $LaSi_{0.5}P_{0.5}$.

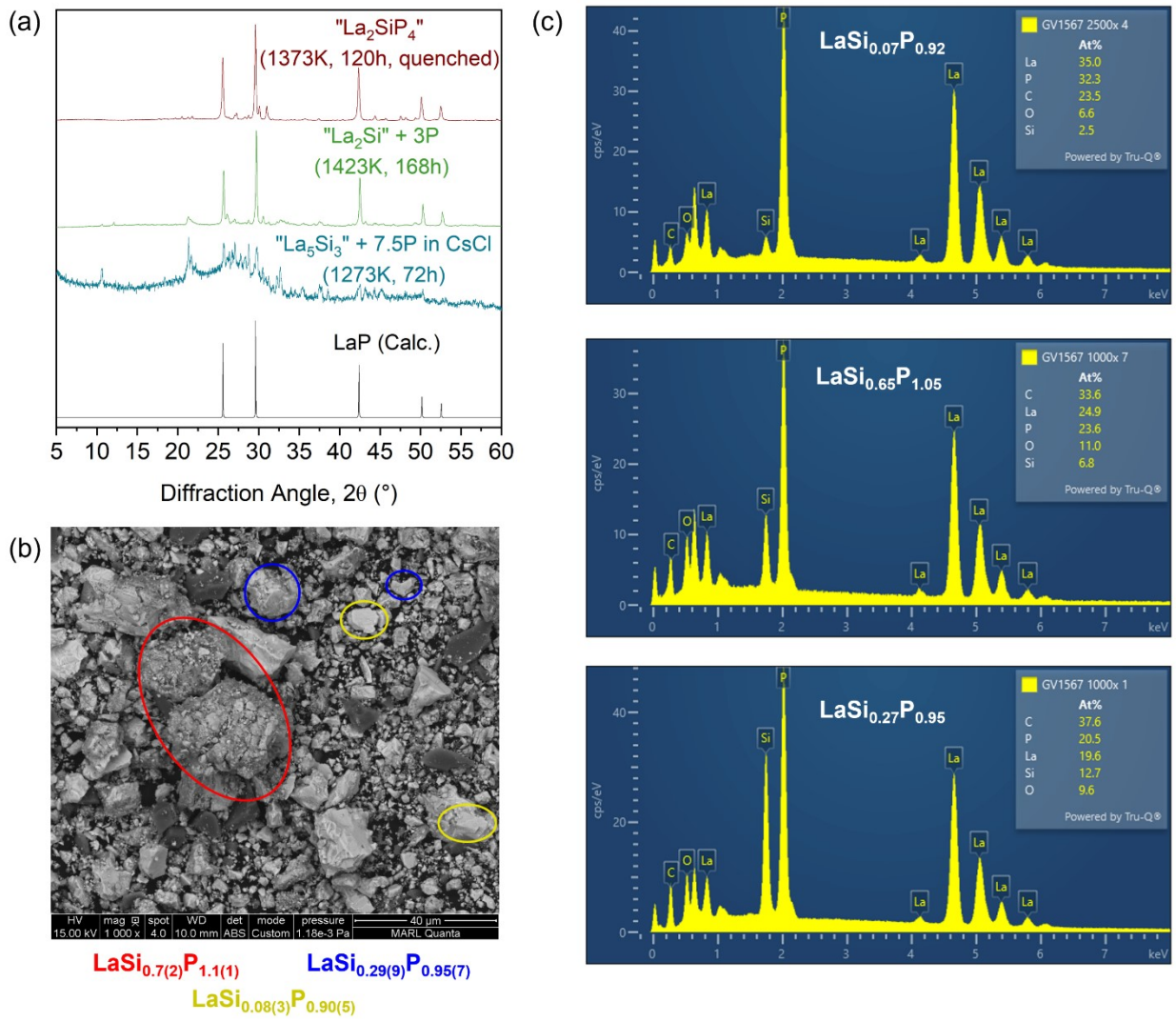

Fig. S2. **(a)** Comparison of experimental PXRD patterns (colored) of selected samples. All 3 samples have unindexed diffraction peaks in addition to LaP (black). **(b)** Backscattered electron SEM image of "La_2SiP_4" sample quenched from 1373 K. Sample powder was mounted on carbon tape for the measurement. Selected regions are highlighted in color with corresponding composition normalized to 1 La. **(c)** Selected EDS spectra for the quenched sample with site compositions normalized to 1 La.

Performance of ANN-ML Potential

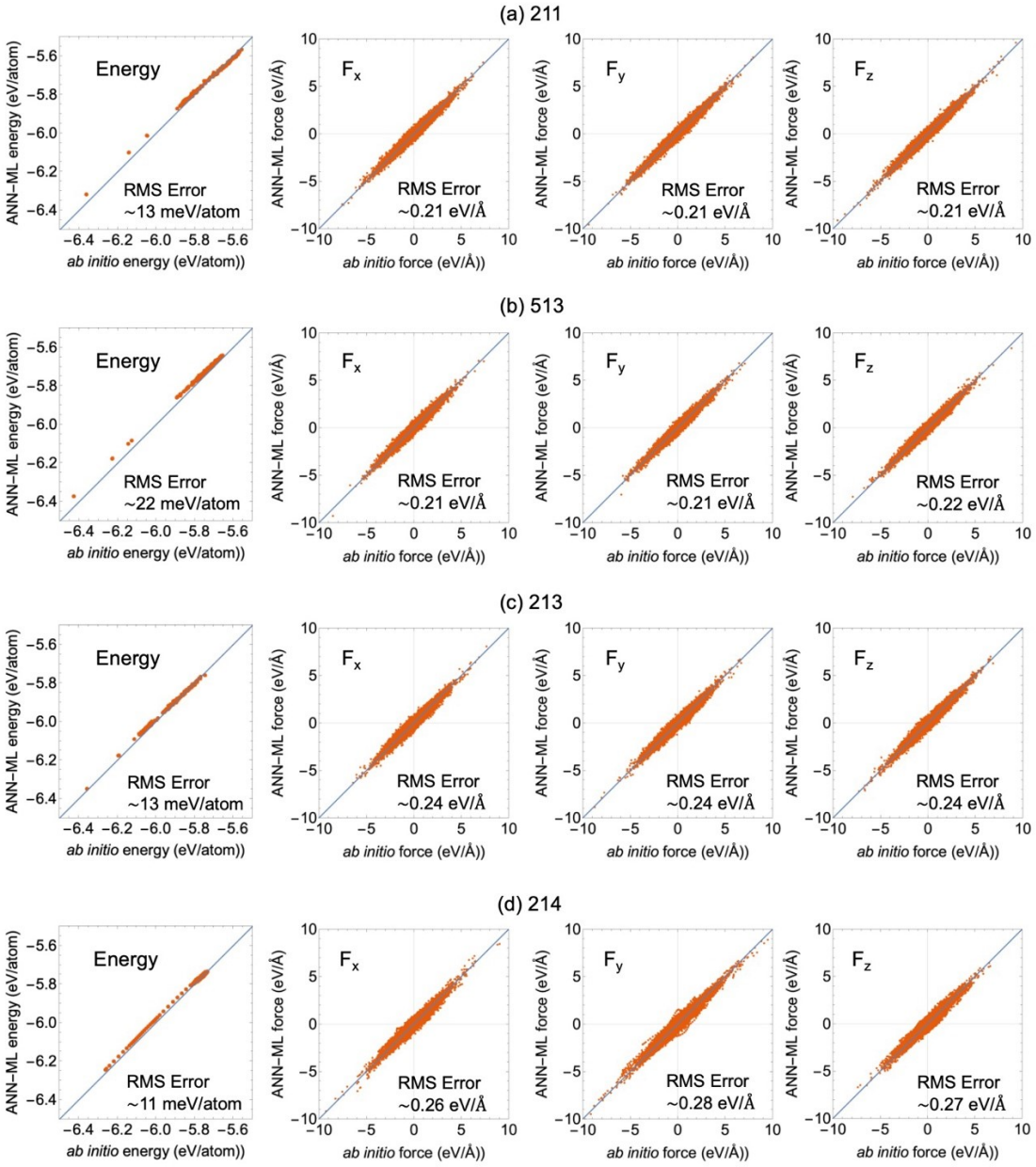

Fig. S3. Potential energy and force predictions by the ANN-ML model for the validation data of **(a)** 211, **(b)** 513, **(c)** 213, and **(d)** 214 phases are compared with *ab initio* calculation results.

Fig. S3 shows the performance of trained ANN-ML potential on the validation dataset of 211, 513, 213, and 214 phases. In order to test the performance of the ANN-ML potential in predicting the crystal growth and melting processes, we collected the DFT results on the melting process of crystals as the validation dataset. In the *ab initio* MD simulations, the supercell crystals were used as the initial structures for the simulations at temperatures (different from the simulation temperatures in the training data) far above the melting points for 3 ps. As shown in **Fig. S3**, the accuracy of total potential energy and force predictions is sufficient for MD simulations.

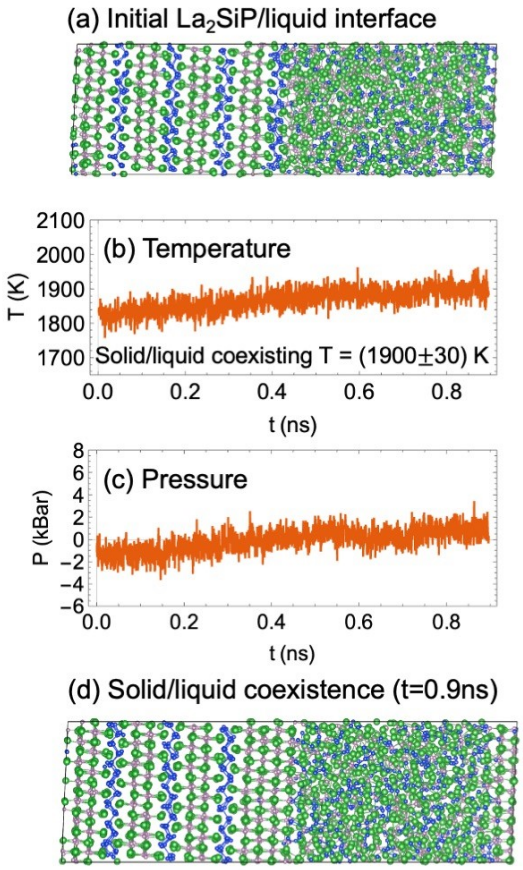

Fig. S4. **(a)** The initial configuration of the La_2SiP/liquid coexistence MD simulation. The evolution of temperature **(b)** and pressure **(c)** in the NVE ensemble simulation are shown. After about 0.5 ns simulation time, the temperature and pressure of system are stable and fluctuate around $T \approx$ 1900K and $P \approx$ 0.7kBar. **(d)** The configuration of the La_2SiP/liquid sample after 0.9 ns simulation time, showing the La_2SiP crystal coexisting with the liquid phase in the stable state of NVE simulation. As such, the melting point of the La_2SiP crystal, i.e., the temperature of solid/liquid equilibrium state, is about 1900K near zero pressure.

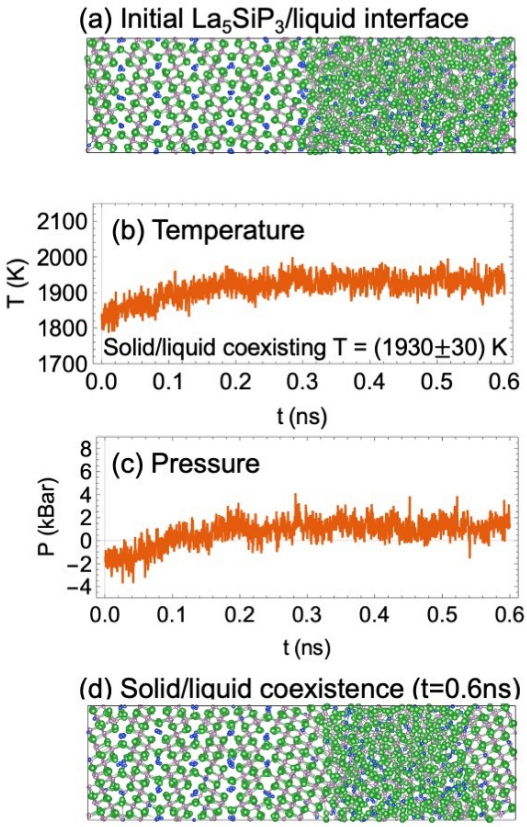

Fig. S5. **(a)** The initial configuration of the La_5SiP_3/liquid coexistence MD simulation. The evolution of temperature **(b)** and pressure **(c)** in the NVE ensemble simulation are shown. After about 0.2 ns simulation time, the temperature and pressure of system are stable and fluctuate around $T \approx$ 1930K and $P \approx$ 1kBar. **(d)** The configuration of the La_5SiP_3/liquid sample after 0.6 ns simulation time, showing the La_5SiP_3 crystal coexisting with the liquid phase in the stable state of NVE simulation. As such, the melting point of the La_5SiP_3 crystal, i.e., the temperature of solid/liquid equilibrium state, is about 1930K near zero pressure.

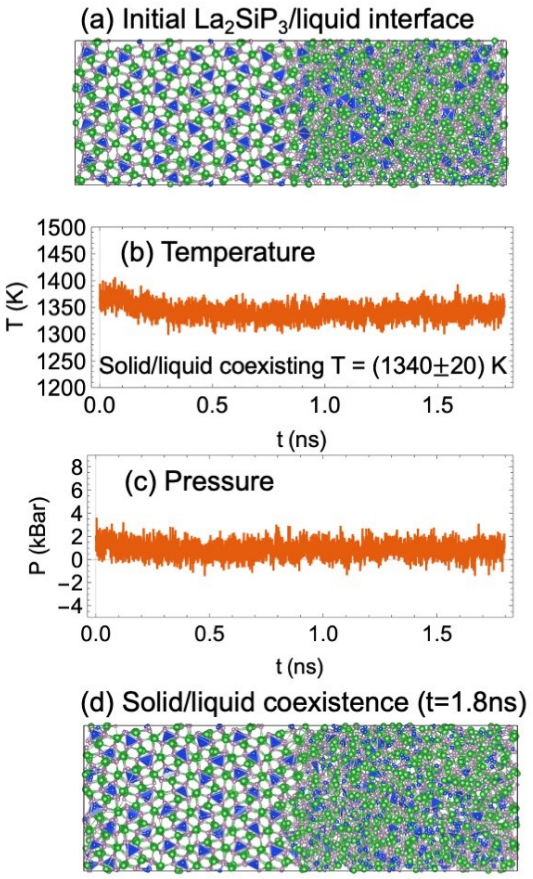

Fig. S6. (a) The initial configuration of the La_2SiP_3/liquid coexistence MD simulation. The evolution of temperature **(b)** and pressure **(c)** in the NVE ensemble simulation are shown. After about 0.5 ns simulation time, the temperature and pressure of system are stable and fluctuate around $T \approx$ 1340K and $P \approx$ 0.9kBar. **(d)** The configuration of the La_2SiP_3/liquid sample after 1.8 ns simulation time, showing the La_2SiP_3 crystal coexisting with the liquid phase in the stable state of NVE simulation. As such, the melting point of the La_2SiP crystal, i.e., the temperature of solid/liquid equilibrium state, is about 1340K near zero pressure.

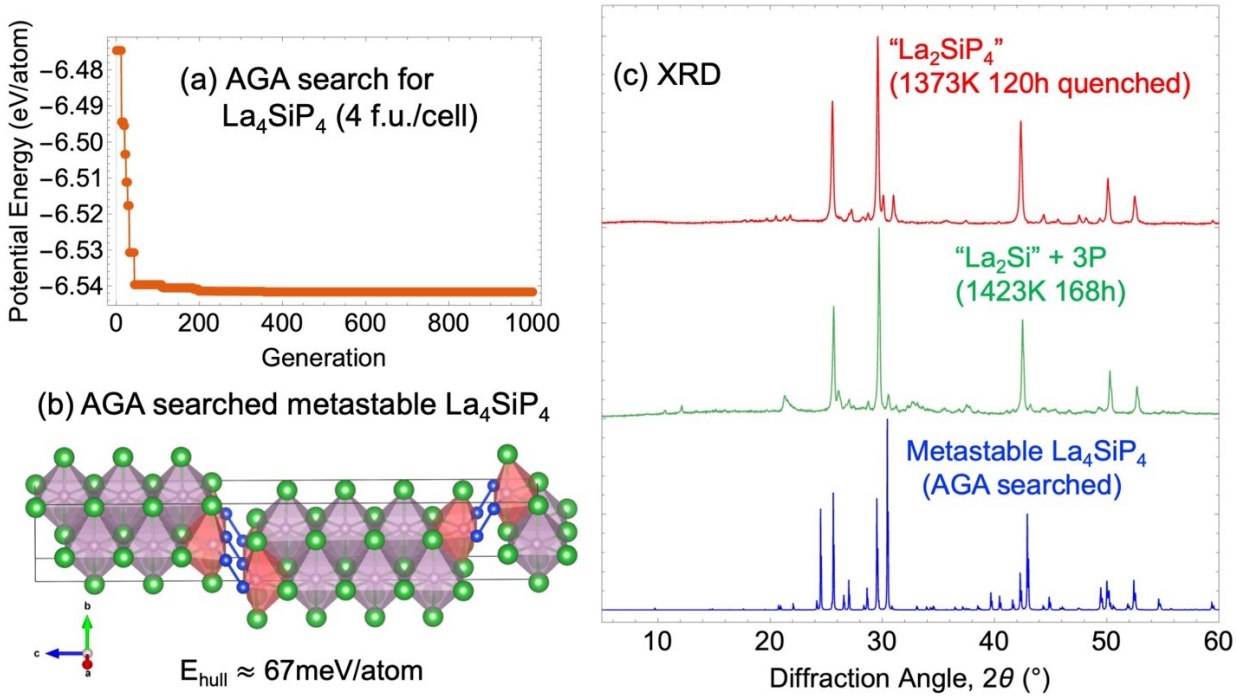

Fig. S7. Adaptive genetic algorithm (AGA) search for low-energy structures of La_4SiP_4 crystal with 4 f.u./cell (total 36 atoms in unit cell). The potential energy vs GA generations plotted in Figure (**a)** shows that the crystalline phase with minimum energy is found since the potential energy doesn't decline for last 500 generations. The obtained metastable La_4SiP_4 structure is plotted in (**b)**, where [P@La_6] octahedra are shown in pink and [P@La_4Si_2] distorted octahedra are shown in red. The LaP slabs which are formed by [P@La_6] octahedra are connected via Si-Si bonds between [P@La_4Si_2] distorted octahedra. Its formation energy calculated by DFT is 67 meV/atom above the convex hull. Comparison of experimental XRD data and the calculated pattern for the AGA searched low-energy La_4SiP_4 structures (blue) is shown in (**c**).

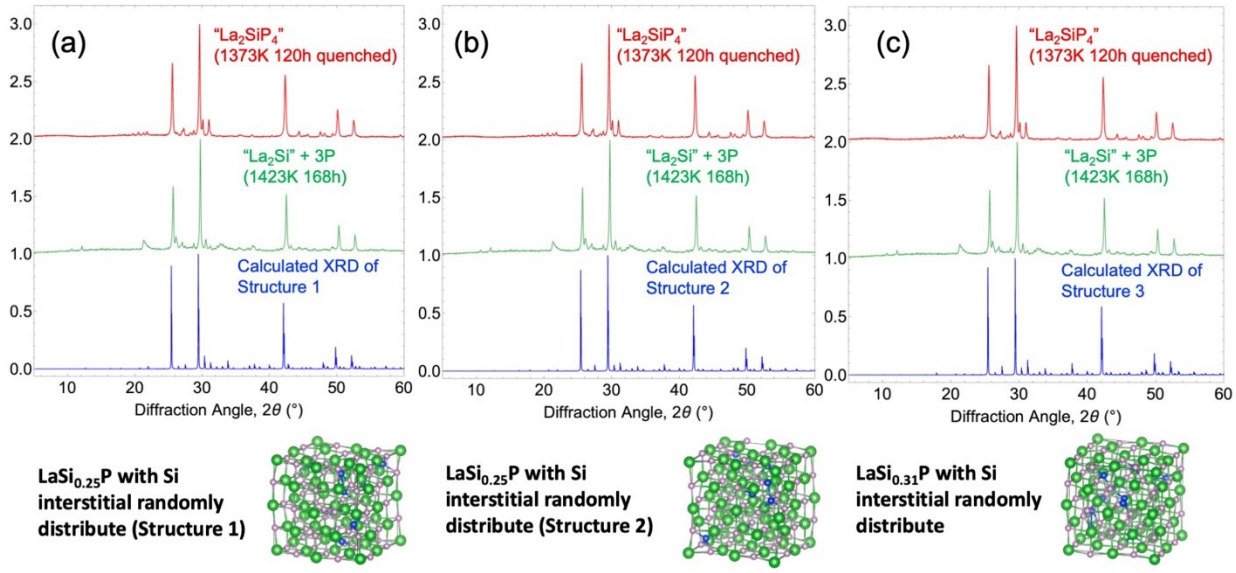

Fig. S8. Comparison of experimental PXRD data with some Si-interstitial LaP model structures. **(a)**, **(b)** Two $LaSi_{0.25}P$ structures. **(c)** $LaSi_{0.31}P$ structure. These La-Si-P phases are modeled by randomly inserting Si atoms into the interstitial site of $2 \times 2 \times 2$ LaP supercell lattice. The calculated XRD patterns of these model structures are given in blue.

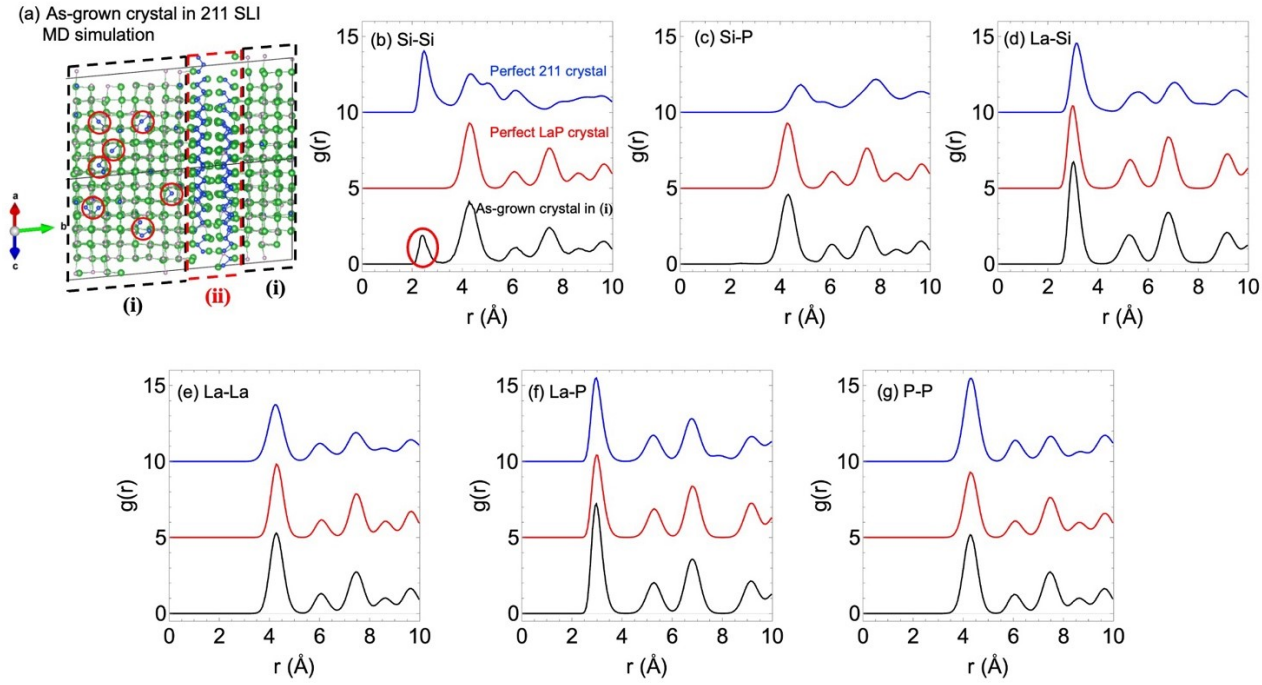

Fig. S9. (a) The as-grown LaP phase in 211 solid-liquid interface (SLI) MD simulation. We observed that the as-grown crystal in the region (i) has the LaP crystal structure, where Si atoms randomly and homogeneously substitute P atoms of LaP_6 octahedron. It also can be seen that the part of 211 crystal have grown in the region (ii). **(b)-(g)** The pair correlation functions (PCFs) of as-grown crystal in region i plotted by black lines, where the red curves denote the PCFs of perfect LaP crystal. Black curves in Figure **(d)** and **(f)** show that $g_{La\text{-}P}(r)$ is the same as $g_{La\text{-}Si}(r)$, while the black curves in Figure **(c)** and **(g)** show $g_{P\text{-}P}(r)$ is also same as $g_{Si\text{-}P}(r)$; this indicates that the Si atoms occupy the site of P atoms in LaP crystal. The black curve in Figure **(b)** shows the PCFs of as-grown crystal in region (i) are close to that of perfect LaP crystal but the peak of $g_{Si\text{-}Si}(r)$ around 2.4Å is absent in LaP crystal. As shown in red circle in **(a)**, this peak corresponds to Si-Si bonds imbedded among La-P octahedron.

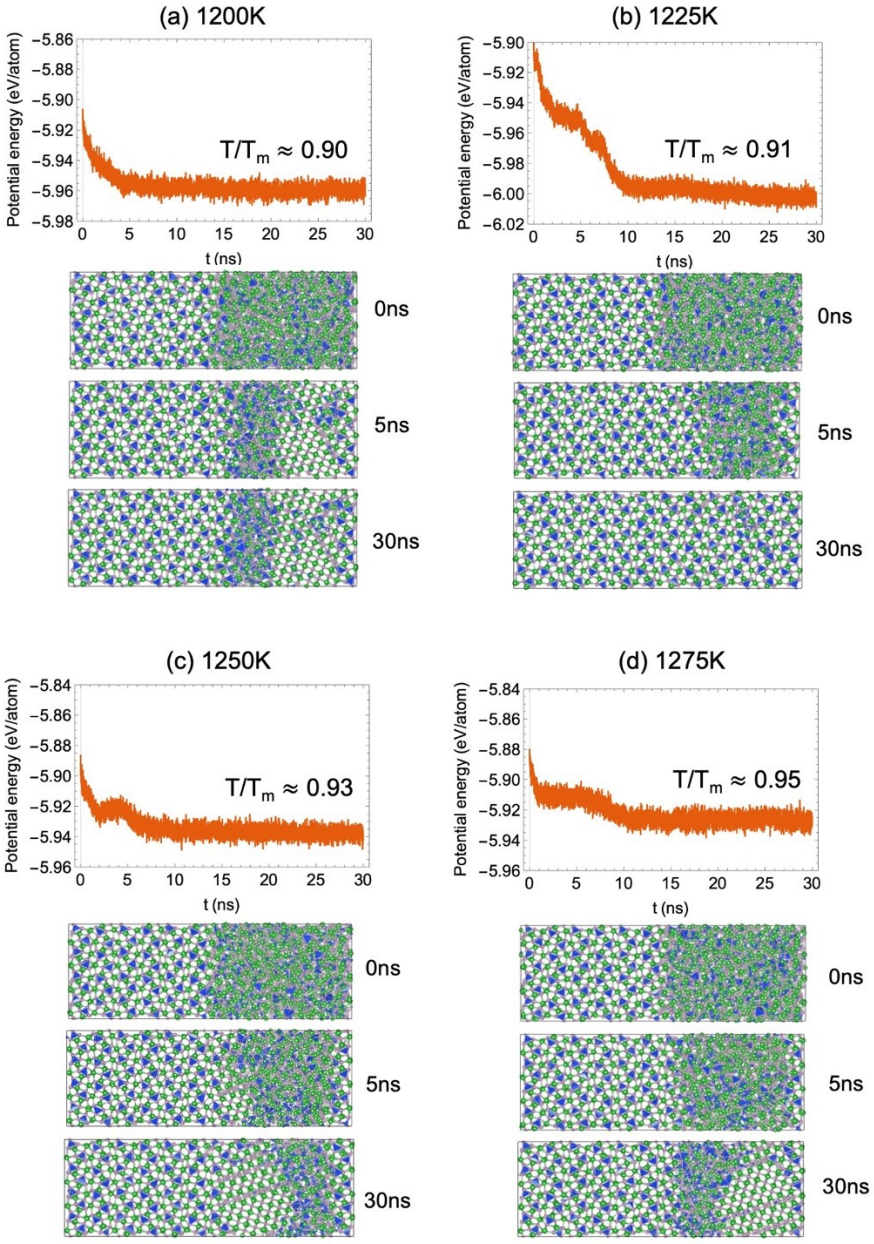

Fig. S10. MD simulation of crystal growth of 213 crystal at 213/liquid interface at temperature **(a)**1200K, **(b)**1225K, **(c)**1250K, and **(d)**1275K, respectively. Figure **(a)**, **(c)**, and **(d)** show that both LaP and 213 phases grown at 213/liquid interface, while only the growth of 213 phase is observed in the simulations at temperature of 1225 K as shown in the Figure **(b)**. These simulation results agree well with the fact that LaP phase constantly emerges in experimental synthesis. These simulations also confirmed the growth of 213 phase at 213/liquid interface above the melting point of 214 phase (1200K), which suggests that there is a narrow temperature window of about 75K where the 213 crystal can grow.